J|A|C|S ARTICLES

Published on Web 02/19/2009

High-Affinity Recognition of Lanthanide(III) Chelate Complexes by a Reprogrammed Human Lipocalin 2

Hyun Jin Kim, Andreas Eichinger, and Arne Skerra*

Lehrstuhl für Biologische Chemie, Technische Universität München, Freising-Weihenstephan, Germany

Received August 29, 2008; E-mail: skerra@wzw.tum.de

Abstract: Human lipocalin 2 (Lcn2), also known as neutrophil gelatinase-associated lipocalin (NGAL), which naturally scavenges bacterial ferric siderophores, has been engineered to specifically bind rare-earth and related metal ions as chelate complexes with [(*R*)-2-amino-3-(4-aminophenyl)propyl]-*trans*-(*S*,*S*)-cyclohexane-1,2-diaminepentaacetic acid (*p*-NH_2-Bn−CHX-A″-DTPA). To this end, 12 amino acid residues in the ligand pocket of Lcn2, which is formed by four loops at the open end of an eight-stranded β-barrel, were subjected to targeted random mutagenesis, and from the resulting library, variants with binding activity for the Me·DTPA group were selected using the method of bacterial phage display. One promising candidate was further developed in several cycles of in vitro affinity maturation using partial random mutagenesis and selection (via phage display and/or *Escherichia coli* colony screening) under conditions of increasing stringency. As result, an Lcn2 variant was obtained that binds Y·DTPA with a dissociation constant as low as 400 pM. The Lcn2 variant specifically recognizes the artificial ligand, as exemplified in (competitive) ELISA and real-time surface plasmon resonance analyses. DTPA-complexed Y^{3+}, Tb^{3+}, Gd^{3+}, and Lu^{3+} are most tightly bound, comprising metal ions whose isotopes are in common use for radiotherapy and imaging. All of the Lcn2 variants are stably folded and can be functionally produced in high yield in *E. coli*. X-ray crystallographic analyses show that the new ligand is well-accommodated in the central cavity of the engineered lipocalin, whose fold is largely preserved, but that the mode of binding differs from the one seen with the natural ligand Fe·enterobactin. This structural study reveals analogies but also differences with respect to previously described antibody−metal chelate complexes. Notably, the functionalized side chain of DTPA protrudes from the ligand pocket of the lipocalin in such a way that its conjugates (with other haptens, for example) are recognized too. With their small sizes and robust fold based on a single polypeptide chain, the engineered Lcn2 variants provide novel modules and/or fusion partners for radionuclide−chelate capturing strategies that bear promise for medical diagnostics and therapy.

Introduction

The lipocalins are a diverse family of small, robust secretory proteins that serve in the transport or storage of poorly soluble or chemically sensitive vitamins, hormones, and metabolites in many organisms.[1] Their fold is dominated by a central β-barrel comprising eight antiparallel strands, which opens to the solvent at one end. There, four structurally variable peptide loops form the entrance to a calyxlike cavity for the often lipophilic ligand.[2] Among the 10−12 members of this family that are found in the human body,[3] lipocalin 2 (Lcn2), also known as neutrophil gelatinase-associated lipocalin (NGAL)[4] and more recently called siderocalin,[5] plays a role in the innate immune defense against bacterial infections by scavenging Fe^{3+} ions bound to certain bacterial siderophores.

Siderophores are highly potent iron chelators that are secreted by pathogenic bacteria in response to limiting iron concentrations,[6] as are found in human body fluids, to allow iron uptake by specialized bacterial import systems.[7,8] It seems that neutrophils release Lcn2 at sites of infection as an antimicrobial strategy. Indeed, the physiological relevance of Lcn2 has been demonstrated in corresponding knockout mice, where this lipocalin was shown to be essential in limiting the spread of bacteria that rely on enterobactin-mediated iron import.[9]

Lcn2 is a 178 amino acid glycoprotein with strong binding activity for the catecholate-type siderophore Fe^{3+}·enterobactin (also called enterochelin), which is characteristic of *Escherichia coli*[10] (Figure 1C). Compared with other lipocalins, Lcn2 exhibits an unusually large ligand pocket. Therein, a cluster of positively charged side chains confers extraordinary affinity for

(1) *Lipocalins*; Åkerström, B., Borregaard, N., Flower, D. A., Salier, J.-S., Eds.; Landes Bioscience: Georgetown, TX, 2006.
(2) Skerra, A. *Biochim. Biophys. Acta* **2000**, *1482*, 337–350.
(3) Breustedt, D. A.; Schönfeld, D. L.; Skerra, A. *Biochim. Biophys. Acta* **2006**, *1764*, 161–173.
(4) Kjeldsen, L.; Cowland, J. B.; Borregaard, N. *Biochim. Biophys. Acta* **2000**, *1482*, 272–283.
(5) Goetz, D. H.; Holmes, M. A.; Borregaard, N.; Bluhm, M. E.; Raymond, K. N.; Strong, R. K. *Mol. Cell* **2002**, *10*, 1033–1043.
(6) Schaible, U. E.; Kaufmann, S. H. *Nat. Rev. Microbiol.* **2004**, *2*, 946–953.
(7) Braun, V.; Braun, M. *Curr. Opin. Microbiol.* **2002**, *5*, 194–201.
(8) Fischbach, M. A.; Lin, H.; Liu, D. R.; Walsh, C. T. *Nat. Chem. Biol.* **2006**, *2*, 132–138.
(9) Flo, T. H.; Smith, K. D.; Sato, S.; Rodriguez, D. J.; Holmes, M. A.; Strong, R. K.; Akira, S.; Aderem, A. *Nature* **2004**, *432*, 917–921.
(10) Raymond, K. N.; Dertz, E. A.; Kim, S. S. *Proc. Natl. Acad. Sci. U.S.A.* **2003**, *100*, 3584–3588.

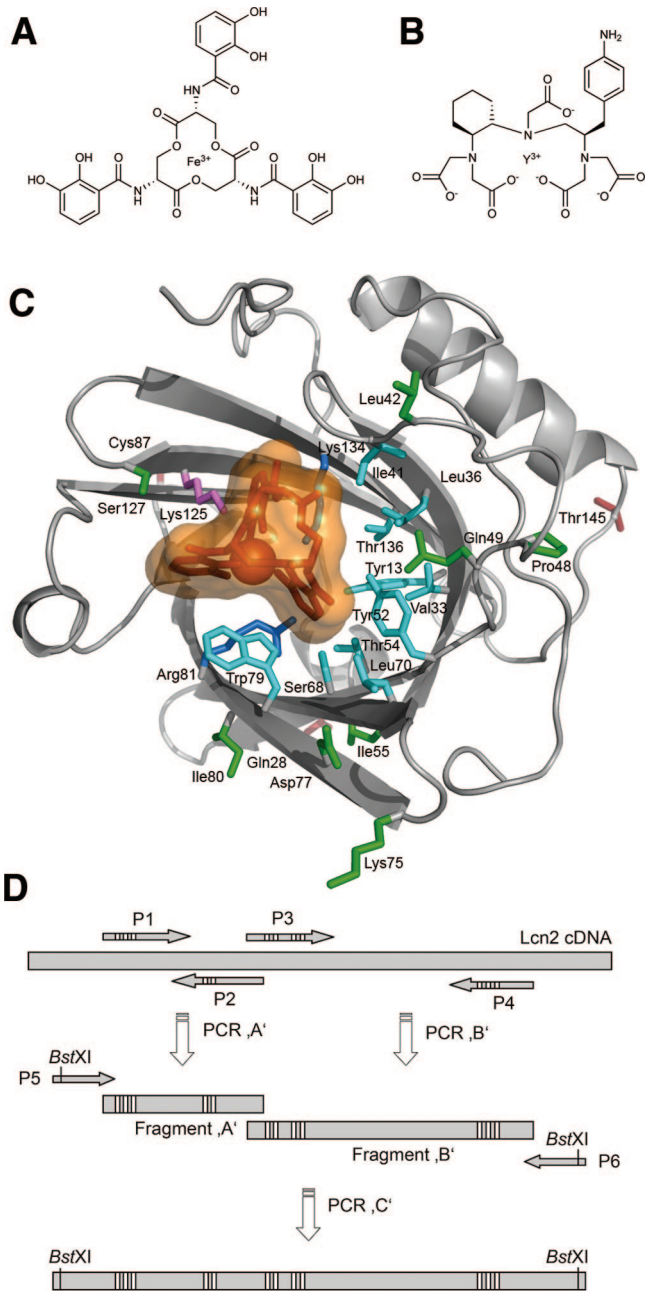

Figure 1. Construction of the random library for selection of Lcn2 variants specific for a new metal chelate. (A, B) Chemical formulas of Fe^{3+}•enterobactin and Y^{3+}•*p*-NH_2-Bn−CHX-A″-DTPA, respectively. (C) Three-dimensional structure of human Lcn2 complexed with Fe^{3+}•enterobactin (PDB entry 1L6M, chain A, here containing the intact ligand; courtesy of Dr. Roland Strong). Side chains randomized in the initial "naive" library are shown in cyan, while the three fixed mutations (see Table 2) are colored red. The three basic side chains R81, K125, and K134, which are involved in π−cation interactions with the catecholate-type ferric siderophore, are shown in blue or violet (for the nonrandomized residue K125). Relevant residues mutated in the course of the subsequent affinity maturation are shown in green. (D) Schematic representation of the PCR assembly strategy for simultaneous randomization of 12 amino acid positions clustered in four regions throughout the primary structure. The previously cloned Lcn2 cDNA was amplified in two parallel PCR reactions: (i) with the degenerate oligodeoxynucleotides P1 and P2 and (ii) with P3 and P4. Randomized positions are indicated by white bars. The two resulting fragments, each covering two mutagenized clusters, were combined and applied as a template in another amplification using the nondegenerate primers P5 and P6. Two noncompatible flanking *Bst*XI restriction sites were applied for subcloning of the gene cassette on pNGAL35, a phasmid vector for phage display.

Table 1. Data Collection and Refinement Statistics

	Tb7.14	Tb7.N9/Y·DTPA−Tris
Crystal Data		
space group	$P4_12_12$	$P4_12_12$
unit cell dimensions *a*, *b*, *c* (Å)[a]	113.59, 113.59, 119.79	82.35, 82.35, 115.13
molecules per asymmetric unit	3	2
Data Collection		
wavelength (Å)	0.95373	0.95373
resolution range (Å)	40.00−2.50 (2.64−2.50)	40.00−2.00 (2.11−2.00)
$I/\sigma(I)$	2.8 (2.0)	4.1 (2.0)
R_{merge} (%)	15.4 (33.1)	10.9 (37.2)
unique reflections	27785	26827
multiplicity	8.7 (8.9)	9.7 (9.8)
completeness	100.0 (100.0)	98.2 (97.4)
Refinement		
R_{cryst}/R_{free}	26.24/29.12	21.33/23.02
protein atoms	4104	2780
ligand atoms	−	98
ion atoms	−	2
solvent atoms	487	328
average *B*-factor (Å^2)	37.85	27.69
Geometry		
rmsd of bond lengths (Å)/ angles (deg)	0.012/1.51	0.0098/1.84
Ramachandran analysis		
core, allowed, generously allowed, disallowed (%)	82.5, 13.4, 2.4, 1.7	88.7, 9.0, 0.7, 1.7

[a] $\alpha = \beta = \gamma = 90°$.

the negatively charged ferric siderophore, with a dissociation constant (K_D) of 0.4 nM,[5] thus allowing effective competition with the bacterial uptake system. Ligand recognition by Lcn2 is rather specific, as it does not bind petrobactin, the siderophore that is crucial for the virulence of *Bacillus anthracis*,[11] or *C*-glycosylated enterobactin analogues such as the salmochelins produced by *Salmonella* spp. and *Klebsiella pneumoniae*.[8] However, this lipocalin also forms stable complexes with bacillibactin from *B. anthracis*,[11] which is chemically related to enterobactin, and with carboxymycobactins from *Mycobacterium tuberculosis*[12] (i.e. siderophores of similar size and shape).

More generally, apart from the need for iron acquisition in biological systems, metal chelate complexes play an increasing role in modern medicine for the purposes of radioimmunotherapy (RIT) and also for in vivo imaging (e.g., radioimmunodiagnosis, RID).[13] Typically, antibodies directed against tumor-specific cell surface markers or peptides specific for disease-related receptors are chemically conjugated to potent synthetic chelating agents,[14] in particular, 1,4,7,10-tetraazacyclododecane-*N*,*N*′,*N*″,*N*‴-tetraacetic acid (DOTA), diethylenetriamine pentaacetic acid (DTPA), and their derivatives. These are then charged with radionuclides of the rare-earth element series, such as Y^{3+} or Lu^{3+}, or similar trivalent metal ions (e.g., In^{3+} or Bi^{3+}). Two radionuclide-conjugated antibodies directed against CD20, Zevalin and Bexxar, have been approved for the therapy of non-Hodgkin's lymphoma, and many antibodies or their fragments are currently subject to further development by

(11) Abergel, R. J.; Wilson, M. K.; Arceneaux, J. E.; Hoette, T. M.; Strong, R. K.; Byers, B. R.; Raymond, K. N. *Proc. Natl. Acad. Sci. U.S.A.* **2006**, *103*, 18499–18503.
(12) Holmes, M. A.; Paulsene, W.; Jide, X.; Ratledge, C.; Strong, R. K. *Structure* **2005**, *13*, 29–41.
(13) Kenanova, V.; Wu, A. M. *Expert Opin. Drug Delivery* **2006**, *3*, 53–70.
(14) Milenic, D. E.; Brady, E. D.; Brechbiel, M. W. *Nat. Rev. Drug Discovery* **2004**, *3*, 488–499.

Table 2. Amino Acid Sequences of Selected Lcn2 Variants[a]

residue no.[b]	Lcn2	Tb7	Tb7.14	Tb7.N9	Tb7.N9.N34	Yd5	C26
28[c]	Gln	His	His	His	His	His	His
87[c]	Cys	Ser	Ser	Ser	Ser	Ser	Ser
145[c]	Thr	Ala	Ala	Ala	Ala	Ala	Ala
33	Val	Gln	Gln	Gln	Gln	Gln	Gln
36	Leu	Arg	Arg	Arg	Arg	Arg	Arg
41	Ile	Ala	Ala	Ala	Ala	Ala	Ala
52	Tyr	Thr	Thr	Thr	Thr	Thr	Thr
54	Thr	[d]Gln	Gln	Gln	Gln	Gln	Gln
68	Ser	Ala	Ala	Ala	Ala	Ala	Ala
70	Leu	Arg	Arg	Arg	Arg	Arg	Arg
79	Trp	Ala	Ala	Leu	Leu	Leu	Leu
81	Arg	Met	Met	Met	Met	Met	Met
134	Lys	Ser	Ser	Ser	Ser	Ser	Ser
136	Thr	Thr	Thr	Thr	Thr	Ser	Ser
138	Tyr	Leu	Leu	Leu	Leu	Leu	Leu
77[e]	Asp	Asp	Asp	Asp	Asp	Glu	Glu
80[e]	Ile	Ile	Thr	Thr	Thr	Thr	Thr
127[e]	Ser	Ser	Ser	Ser	Gln	Gln	Gln
42[f]	Leu	Leu	Leu	Leu	Leu	Leu	Pro
48[f]	Pro	Pro	Pro	Pro	Pro	Pro	Leu
49[f]	Gln	Gln	Gln	Gln	Gln	Gln	Leu
55[f]	Ile	Ile	Ile	Ile	Ile	Ile	Thr
75[f]	Lys	Lys	Lys	Lys	Lys	Lys	Met

[a] Underlined residues denote mutations that were acquired during the preceding affinity maturation cycle. [b] Sequential numbering of the mature protein sequence (see SwissProt entry P80188). [c] Positions 28, 87, and 145 were specifically mutated for reasons of genetic manipulation (see Materials and Methods). [d] The amber stop codon was translated as Gln in the *sup*E background of the bacterial strains used for the selection experiments and was later replaced by the codon CAG via site-directed mutagenesis. [e] Accidental mutations at positions that were not part of the initial random mutagenesis. [f] Mutations arising from error-prone PCR with nucleotide analogues and 9°N_m DNA polymerase.

protein engineering for improved pharmacokinetics and tumor-to-background ratio.[13]

A major obstacle of humanized antibodies for nuclear medicine is their long circulation time, which leads to low contrast for imaging and limited tumor specificity during RIT or RID. To circumvent this problem, so-called pretargeting strategies have been developed, where the tumor-targeting antibody is uncoupled from the chelated radionuclide.[15] This enables the slow process of antibody localization and clearance from circulation in the first stage, prior to the fast and specific delivery of the small-molecule radioactive payload in the second stage. Initially, antibody−streptavidin conjugates were applied in conjunction with biotinylated radionuclide chelates, and later, bispecific antibodies together with chelate complexes conjugated to cognate epitope peptides were used. Moreover, monoclonal antibodies that can directly bind the metal chelate have been developed.[16,17]

The ideal system, however, would be a small metal-chelate-specific binding protein comprising a single polypeptide chain and having robust folding properties that can simply be coupled via gene fusion to a targeting peptide/protein module of choice, such as a natural receptor ligand, an antibody fragment,[13] or an alternative binding protein.[18] Lcn2 offers interesting benefits in this respect. It is an abundant human plasma protein whose concentration normally is ~80 μg/L but can increase up to 10-fold upon bacterial infections,[19] and its single N-linked glycosylation site is dispensable for folding.[20] Furthermore, several members of the lipocalin family have already been successfully engineered for novel ligand specificities as so-called anticalins,[21] including production as functional fusion proteins with various partner domains.

In the present study, we set out to engineer Lcn2 as a binding module for a radionuclide chelate complex. We chose a DTPA derivative complexed with lanthanide ions as the target ligand because this chelator can be quickly charged under physiological buffer conditions, prevents the release of the free metal ion as well as related kidney toxicity, is already in clinical use for antibody conjugates such as Zevalin, and even allows the preparation of two-headed reagents to achieve more sophisticated avidity effects.[22] In particular, the conformationally stabilized derivative cyclohexyl-DTPA (CHX-A″-DTPA)[23] (Figure 1B) forms complexes that are as inert as the ones known for DOTA but more readily takes up the metal ion, and it has been applied in the preparation of stable ^{111}In and ^{90}Y radioconjugates with the anti-Her2 antibody Herceptin,[24] among others. We present here the selection of Lcn2 variants with high affinities for this payload, together with their X-ray crystallographic analysis, which provides insights into the mechanisms of metal chelate recognition by a protein and reveals a mode of binding distinct from that for the natural ligand enterobactin.

Materials and Methods

Preparation of Me·DTPA Complex Conjugates. A 365 nmol (5 mg) sample of bovine pancreatic ribonuclease A (RNase A; Fluka Chemie, Buchs, Switzerland), which exhibits up to 10 Lys side chains as well as its N-terminus for covalent coupling, was dissolved in 1 mL of 100 mM $NaHCO_3$ (>99.5%, Carl Roth, Karlsruhe, Germany) (pH 8.3) and reacted with a solution of 1.8 μmol (1.28 mg) of [(*R*)-2-amino-3-(4-isothiocyanatophenyl)propyl]-*trans*-(*S*,*S*)-cyclohexane-1,2-diaminepentaacetic acid·3HCl (*p*-SCN-Bn−CHX-A″-DTPA; Macrocyclics, Dallas, TX) in 10 μL of DMSO overnight at 4 °C under agitation. Typically, under these conditions, one activated DTPA group per protein molecule reacted, as quantified by electrospray ionization mass spectrometry (ESI-MS; QtoF Ultima Global, Waters, Eschborn, Germany). Similarly, 150 nmol (10 mg) of bovine serum albumin (BSA; Sigma-Aldrich, Munich, Germany) was coupled with 750 nmol (528 μg) of *p*-SCN-Bn−CHX-A″-DTPA. For removal of excess reagent and buffer exchange, a gel filtration on a PD-10 column (Amersham Pharmacia Biotech, Freiburg, Germany) was performed with 0.1 M ammonium acetate (>99.9%, Sigma-Aldrich)/acetic acid (pH 5).[25] Next, an equimolar solution (with respect to the carrier protein) of $TbCl_3$, YCl_3, $LuCl_3$, $GdCl_3$, or $InCl_3$ (all from Sigma-Aldrich) in the same ammonium acetate buffer was added, and after incubation for 10 min at room temperature, the resulting conjugate was stored at −80 °C. With this procedure, a Me·DTPA−RNase conjugate with average 1:1:1 stoichiometry was obtained, as confirmed by fluorescence titration of a sample of the gel-filtrated DTPA−RNase with the gravimetri-

(15) Chang, C. H.; Sharkey, R. M.; Rossi, E. A.; Karacay, H.; McBride, W.; Hansen, H. J.; Chatal, J. F.; Barbet, J.; Goldenberg, D. M. *Mol. Cancer Ther.* **2002**, *1*, 553–563.
(16) Le Doussal, J. M.; Gruaz-Guyon, A.; Martin, M.; Gautherot, E.; Delaage, M.; Barbet, J. *Cancer Res.* **1990**, *50*, 3445–3452.
(17) Corneillie, T. M.; Whetstone, P. A.; Fisher, A. J.; Meares, C. F. *J. Am. Chem. Soc.* **2003**, *125*, 3436–3437.
(18) Skerra, A. *Curr. Opin. Biotechnol.* **2007**, *18*, 295–304.
(19) Xu, S.; Venge, P. *Biochim. Biophys. Acta* **2000**, *1482*, 298–307.
(20) Coles, M.; Diercks, T.; Muehlenweg, B.; Bartsch, S.; Zolzer, V.; Tschesche, H.; Kessler, H. *J. Mol. Biol.* **1999**, *289*, 139–157.
(21) Skerra, A. *Curr. Opin. Mol. Ther.* **2007**, *9*, 336–344.
(22) Gruaz-Guyon, A.; Janevik-Ivanovska, E.; Raguin, O.; De Labriolle-Vaylet, C.; Barbet, J. *Q. J. Nucl. Med.* **2001**, *45*, 201–206.
(23) Brechbiel, M. W.; Gansow, O. A. *J. Chem. Soc., Perkin Trans. 1* **1992**, 1173–1178.
(24) Blend, M. J.; Stastny, J. J.; Swanson, S. M.; Brechbiel, M. W. *Cancer Biother. Radiopharm.* **2003**, *18*, 355–363.
(25) Wu, C.; Kobayashi, H.; Sun, B.; Yoo, T. M.; Paik, C. H.; Gansow, O. A.; Carrasquillo, J. A.; Pastan, I.; Brechbiel, M. W. *Bioorg. Med. Chem.* **1997**, *5*, 1925–1934.

cally prepared $TbCl_3$ solution, which revealed an easily detectable increase in Tb luminescence (λ_{ex} = 295 nm, λ_{em} = 545 nm; FluoroMax-3, Jovin Yvon, Longjumeau, France) until saturation was achieved.

A double conjugate of RNase (or BSA) with DTPA and digoxigenin (DIG) was prepared by first reacting 915 nmol of *p*-SCN-Bn−CHX-A″-DTPA in 10 μL of DMSO with 183 nmol of the carrier protein dissolved in 970 μL of 100 mM $NaHCO_3$ (pH 8.3) overnight at 4 °C and then adding 366 nmol of digoxigenin-3-*O*-methylcarbonyl-ε-aminocaproic acid *N*-hydroxysuccinimide ester (DIG-NHS; Roche Diagnostics, Mannheim, Germany) in 20 μL of DMSO. This mixture was allowed to stand for 1 h at room temperature, after which gel filtration and complex formation with the metal ion were carried out as described above.

An Y·DTPA−Tris conjugate was prepared by incubating 528 μg (750 nmol) of *p*-SCN-Bn−CHX-A″-DTPA in 100 μL of 100 mM tris(hydroxymethyl)aminomethane (Tris; >99.9%, AppliChem, Darmstadt, Germany)/HCl (pH 8.0) overnight at room temperature (to achieve thiourea formation) and then adding 227 μg (750 nmol) of YCl_3.

A direct conjugate of Me·DTPA with DIG-NHS was prepared by dissolving 2 μmol of [(*R*)-2-amino-3-(4-aminophenyl)propyl]-*trans*-(*S*,*S*)-cyclohexane-1,2-diaminepentaacetic acid·4HCl (*p*-NH_2-Bn−CHX-A″-DTPA; Macrocyclics) in 100 μL of DMF with the addition of 1.7 μL (12 μmol) of diisopropylethylamine (Fluka) and reacting it with 2 μmol of DIG-NHS overnight at room temperature. A 10 μL aliquot of this solution was diluted with 980 μL of the ammonium acetate buffer, and 10 μL of a 20 mM YCl_3 or $TbCl_3$ solution in the same buffer was added.

Construction of a Mutant Lcn2 Phage Display Library. A combinatorial library of Lcn2 variants was generated on the basis of the cloned cDNA,[3] which carried the amino acid substitution Cys87Ser to remove the single unpaired thiol side chain[26] and the substitutions Gln28His and Thr145Ala to introduce two unique *Bst*XI restriction sites with noncompatible overhangs, thus permitting unidirectional cloning of the mutagenized central gene cassette. Mutagenesis and polymerase chain reaction (PCR) assembly of this region were performed according to a published strategy[27,28] in two steps (Figure 1D): First, two DNA fragments were separately amplified using pairs of degenerate oligodeoxynucleotides P1 (5′-CAA TTC CAT GGG AAG TGG TAT YNS GTA GGT YNS GCA GGG AAT GCA NNS CTC AGA GAA GAC AAA GAC CCG CA-3′) and P2 (5′-GTG ACA TTG TAG CTC TTA TCT TCT TTC AGC TCA TAG ATS NRG GCS NNC ATC TTT TGC GGG TCT TTG TCT TC-3′) as well as P3 (5′-AAG AGC TAC AAT GTC ACA NNS GTC NNS TTT AGG AAA AAG AAG TGT GAC TAC NNS ATC NNS ACT TTT GTT CCA GGT TCC C-3′) and P4 (5′-GCC AGC TCC TTG GTT CTC CCS NRG AGS NRG ATS NNG AAG TAC TCC CTG TTT TGA G-3′), which cover the amino acid positions 33/36/41, 52/54, 68/70/79/81, and 134/136/138, respectively. Second, the two resulting PCR products were isolated by agarose gel electrophoresis[29] and mixed in the presence of the two flanking primers P5 (5′-CCA GGA CAA CCA ATT CCA TGG GAA GTG G-3′) and P6 (5′-GTT CCG AAG CCA GCT CCT TGG TTC TC-3′), after which a few cycles of PCR were performed to assemble and amplify the full-length central gene cassette. All of the PCR steps were performed using *Taq* DNA polymerase (Fermentas MBI, St. Leon-Roth, Germany) as described elsewhere.[30] Oligodeoxynucleotides were purchased in HPLC grade from Thermo Fisher Scientific (Ulm, Germany) and further purified by urea PAGE as necessary. The resulting DNA library was cut with *Bst*XI (Promega, Mannheim, Germany) and cloned on the phagemid vector pNGAL35, which is based on the generic expression vector pASK75[31] and codes for a fusion protein composed of the *Omp*A signal peptide, T7-tag, the modified mature Lcn2 followed by an amber stop codon, and the C-terminal fragment of the gene III coat protein of the filamentous bacteriophage M13 (i.e., similar to what was previously described[27,28] for the bilin-binding protein). After electroporation of *E. coli* XL1-Blue[32] with the ligation mixture of 6 μg of PCR product and 56 μg of digested plasmid DNA, ~6.5×10^{10} transformants were obtained.

Selection of Lcn2 Variants by Phage Display and Colony Screening. For production of recombinant phagemids, a culture of *E. coli* XL1-Blue transformed with the pNGAL35 library was infected with VCS-M13 helper phages (Stratagene, Amsterdam Zuidoost, The Netherlands), whereby biosynthesis of the Lcn2-pIII fusion protein was induced with 25 μg/L anhydrotetracycline (Acros, Geel, Belgium) following published protocols.[27,30]

For each panning cycle, ~10^{12} recombinant phagemids in PBS (4 mM KH_2PO_4, 16 mM Na_2HPO_4, 115 mM NaCl, pH 7.4) were incubated for 1 h with ImmunoSticks (Nunc, Wiesbaden, Germany) that had been coated with 100 μg/mL Tb·DTPA−RNase conjugate and blocked for 2 h with 1.2 mL of blocking buffer [PBS containing 0.1% (v/v) Tween 20 (polyoxyethylene sorbitan monolaurate; AppliChem) and 2% (w/v) BSA]. After eight washing steps with PBS/T [PBS containing 0.1% (v/v) Tween 20], bound phagemids were eluted for 15 min with 0.1 M glycine/HCl (pH 2.2) and then immediately neutralized with 0.5 M Tris base. The phagemids were titered and reamplified prior to the next panning. After 7 cycles, an enrichment of the acid-eluted phagemids by a factor of 1000 compared to the phagemid number after the first cycle was observed.

The pooled phasmid preparation from the last panning step was used to subclone the mutagenized gene cassette via *Bst*XI on the plasmid pNGAL38, which encodes a fusion of the *Omp*A signal peptide and the Lcn2 with the C-terminal *Strep*-tag II,[33] followed by an amber stop codon as well as a gene for the albumin-binding domain (ABD) from streptococcal protein G.[30] Next, a filter sandwich colony screening assay was performed, whereby the Lcn2-ABD fusion proteins were released from the live colonies plated on a hydrophilic filter membrane and became functionally captured on an underlying second membrane coated with human serum albumin (HSA).[30] This membrane was probed with 150 nM Tb·DTPA−BSA−DIG (or with the corresponding RNase conjugate) in PBS/T for 1 h followed by development with an anti-DIG Fab/alkaline phosphatase (AP) conjugate (Roche Diagnostics) and chromogenic staining as described elsewhere.[30] After spots with intense color signals on this membrane were identified, the corresponding colonies were picked from the first filter and propagated for plasmid isolation and/or side-by-side comparison in a secondary colony screen. During this step, DTPA conjugates not charged with a metal ion served as negative control, and to avoid erroneous signals arising from trace metal ion contamination, a high purity 0.1 M ammonium acetate buffer (>99.9%, pH 7.1) was used.

For the subsequent improvement of the affinity of the initially selected Lcn2 variant Tb7, the corresponding *Bst*XI cassette was subjected to error-prone PCR, as described below, followed by phagemid display. In this case, 10^{11} recombinant phagemids were incubated for 1 h with ImmunoSticks that had been coated with 25 μg/mL Tb·DTPA−RNase conjugate for the first cycle and 10 μg/mL Tb·DTPA−RNase conjugate for the second to fourth cycles.

For affinity maturation of the Lcn2 variant Yd5, the corresponding *Bst*XI cassette was subjected to error-prone PCR (see below)

(26) Goetz, D. H.; Willie, S. T.; Armen, R. S.; Bratt, T.; Borregaard, N.; Strong, R. K. *Biochemistry* **2000**, *39*, 1935–1941.
(27) Beste, G.; Schmidt, F. S.; Stibora, T.; Skerra, A. *Proc. Natl. Acad. Sci. U.S.A.* **1999**, *96*, 1898–1903.
(28) Skerra, A. *J. Biotechnol.* **2001**, *74*, 257–275.
(29) Sambrook, J.; Russel, D. W. *Molecular Cloning: A Laboratory Manual*, 3rd ed.; Cold Spring Harbor Laboratory Press: Cold Spring Harbor, NY, 2001.
(30) Schlehuber, S.; Beste, G.; Skerra, A. *J. Mol. Biol.* **2000**, *297*, 1105–1120.
(31) Skerra, A. *Gene* **1994**, *151*, 131–135.
(32) Bullock, W. O.; Fernandez, J. M.; Short, J. M. *Biotechniques* **1987**, *5*, 376–378.
(33) Schmidt, T. G.; Skerra, A. *Nat. Protoc.* **2007**, *2*, 1528–1535.

that was again followed by phagemid display, this time under conditions of limiting off-rate. To this end, 10^{12} phagemids were incubated for 1 h with ImmunoSticks coated with 10 μg/mL Y·DTPA−RNase conjugate. After five washing steps, the sticks were incubated with 800 μL of a 500 μM solution of the free metal chelate complex Y·*p*-NH_2-Bn−CHX-A″-DTPA in PBS for 30 min at room temperature to achieve competition. After another three washing steps with PBS, remaining bound phagemids were eluted under acid conditions as described above. In this case, three selection cycles were carried out in total.

For some of the affinity maturation steps, the mutagenized Lcn2 libraries were directly applied to the colony screen, yet under increasingly stringent conditions, by decreasing the concentration of the Tb/Y·DTPA−RNase−DIG conjugate from 50 to 5 nM. To raise the stringency even further, the strictly monovalent Tb/Y·DTPA−DIG small-molecule conjugate was applied at concentrations of 20 to 1 nM. Finally, a competitive colony screen was performed by incubating the second membrane first for 1 h with 10 nM Y·DTPA−DIG and then, after washing three times with PBS/T, for 1 h with 10 μM plain complex Y·*p*-NH_2-Bn−CHX-A″-DTPA, followed by washing, detection, and staining as described above.

Targeted Random Mutagenesis of Amino Acid Subsets in Lcn2 Variants. For randomization of positions 79 and 80, primers P5 and mut79back (5′-GGA ACC TGG AAC AAA AGT CAT SNN SNN GTA GTC AC A CTT CTT-3′) were applied in a PCR with *Taq* DNA polymerase as above using pNGAL15-Tb7 as the template. A second PCR fragment was generated using primers mut79for (5′-GAC TTT TGT TCC AGG TTC C-3′) and P6. Both fragments were assembled using the flanking primers P5 and P6. To randomize positions 125 and 134, primers P5 and mut134back (5′-GCC AGC TCC TTG GTT CTC CCG AGG AGG GTG ATS NNG AAG TAC TCC CTG TTT TGA GAA ACS NNC TTG AAG AAC ACC-3′) were applied using pNGAL15-Tb7 as the template. The PCR product was extended to full length via reamplification with primers P5 and P6. To randomize positions 125 and 127, primers P5 and mut127back (5′-GCC AGC TCC TTG GTT CTC CCG AGG AGG GTG ATG GAG AAG TAC TCC CTG TTT TGS NNA ACS NNC TTG AAG AAC ACC-3′) were applied using pNGAL15-Tb7.N9 as the template. The PCR product was again extended to full length via reamplification with primers P5 and P6. To randomize positions 77 and 136, primers P5 and mut77back (5′-GGA ACC TGG AAC AAA AGT CAT GGT CAG GTA SNN ACA CTT CTT TTT CCT AAA CCT G-3′) were applied using pNGAL15-Tb7.N9.N34 as the template. In this case, a second PCR fragment was generated using primers mut79for and mut136back (5′-GCC AGC TCC TTG GTT CTC CCG AGG AGS NNG ATG GAG AAG TAC TCC CT-3′). Again, the two fragments were assembled using the primers P5 and P6. To simultaneously randomize positions 33, 54, and 136, primers mut33for (5′-CAA TTC CAT GGG AAG TGG TAT NNS GTA GGT CGG GCA GGG-3′) and mut54back (5′-CTT CTT TCA GCT CAT AGA TSN NGG CGG TCA TCT TTT GCG G-3′) were applied using pNGAL15-Tb7.N9.N34 as the template. A second PCR fragment was generated using primers mut136for (5′-ATC TAT GAG CTG AAA GAA G-3′) and mut136back. Once again, both PCR fragments were assembled with the flanking primers P5 and P6. In each case, the mutagenized DNA fragment was subcloned on pNGAL38 for subsequent colony screening.

Lcn2 Mutagenesis by Error-Prone PCR. The construction of a second-generation mutant library was carried out by PCR of the gene encoding Tb7, cloned on pNGAL15, with dNTP analogues.[34] The 20 μL reaction mixture contained 10 ng of template DNA, the dNTP analogues 8-oxo-2′-deoxyguanosine-5′-triphosphate (8-oxo-dGTP) and 6-(2-deoxy-β-D-ribofuranosyl)-3,4-dihydro-8*H*-pyrimido-[4,5-*c*][1,2]-oxazin-7-one-5′-triphosphate (dPTP) (each 25 μM; both from TriLink, San Diego, CA), 500 μM conventional dNTPs, 0.5 μM flanking primers P5 and P6, 2 mM $MgCl_2$, and 2.5 units of *Taq* DNA polymerase. Ten cycles were carried out at temperatures of 92 °C for 1 min, 55 °C for 1.5 min, and 72 °C for 5 min, after which reamplification was performed with 5 μL of the sample from above in a 100 μL setup using 20 cycles under the same conditions but omitting the analogues.

Randomization of the variant Yd5 was similarly performed by error-prone PCR using primers P5 and P6 in the presence of 50 μM dPTP, 50 μM 8-oxo-dGTP, and 1 unit of 9°N_m DNA polymerase (New England Biolabs, Frankfurt am Main, Germany) and subsequent reamplification as described above. The PCR products were purified by agarose gel electrophoresis,[29] cut with *Bst*XI, and subcloned on pNGAL35 for phagemid display selection.

Soluble Protein Production and Purification. The recombinant Lcn2 and its variants were produced in a functional state by periplasmic secretion in *E. coli* as previously described.[3] The strain BL21[35] or the *sup*E strain TG1-F$^-$ (a derivative of *E. coli* K12 TG1[36] that had been cured from its episome using acridine orange[37]) was used, each transformed with the vectors pNGAL14[3] and pNGAL15 for the wild-type Lcn2 and its variants, respectively. Both plasmids encode a fusion of the *Omp*A signal peptide with the mature protein and the C-terminal *Strep*-tag II, whereby the latter vector carries the two noncompatible *Bst*XI restriction sites for unidirectional subcloning of the mutated gene cassette. The soluble protein was affinity-purified by means of the *Strep*-tag II[33] followed by size-exclusion chromatography (SEC) on a Superdex 75 HR 10/30 column (Amersham) in the presence of PBS. Protein purity was checked by SDS-PAGE,[38] and protein concentrations were determined by absorption measurements at 280 nm using calculatory extinction coefficients of 29 930 M^{-1} cm^{-1} for wtLcn2 and 21 680 M^{-1} cm^{-1} for its variants Tb7, Tb7.14, Tb7.N9, Tb7.N9.N34, Yd5, and C26.[39]

Measurement of Binding Activity for the Me·DTPA Group in an ELISA. For selective capture of the Lcn2 variants carrying the C-terminal *Strep*-tag II,[33] a 96-well MaxiSorp polystyrene microtiter plate (Nunc) was coated with 50 μL of 1.8−10 μg/mL *Strep*MAB-Immo (IBA, Göttingen, Germany) in PBS overnight at 4 °C and blocked with 1% (w/v) BSA in PBS/T at room temperature for 1 h. After three washing steps with PBS/T, 50 μL of a 50–250 nM solution of the purified Lcn2 variant was applied for 1 h to every well. After another wash, 50 μL of a dilution series of the Me·DTPA−RNase−DIG conjugate was added and incubated for 1 h. The wells were washed again, and bound conjugate was detected using treatment for 1 h with 50 μL of anti-DIG Fab/AP conjugate diluted 1:1000 in PBS/T followed by signal development in the presence of 100 μL of 0.5 mg/mL *p*-nitrophenyl phosphate in 100 mM Tris/HCl (pH 8.8) containing 100 mM NaCl and 5 mM $MgCl_2$. The time course of absorption, $\Delta A/\Delta t$, at 405 nm was measured in a SpectraMax 250 reader (Molecular Devices, Sunnyvale, CA), and KaleidaGraph software (Synergy Software, Reading, PA) was used to fit the data to the equation

$$\dot{A} = \dot{A}_{max} \frac{[L]_{tot}}{K_D + [L]_{tot}}$$

in which $[L]_{tot}$ represents the concentration of the applied ligand conjugate and K_D is the dissociation constant.[40]

Alternatively, a competitive enzyme-linked immunosorbent assay (ELISA) was performed in a similar manner, employing the Me·DTPA−RNase−DIG conjugate at a fixed concentration of 2.5−5 nM in the presence of varying concentrations of the free

(34) Zaccolo, M.; Williams, D. M.; Brown, D. M.; Gherardi, E. *J. Mol. Biol.* **1996**, *255*, 589–603.
(35) Studier, F. W.; Moffatt, B. A. *J. Mol. Biol.* **1986**, *189*, 113–130.
(36) Gibson, T. J. Cambridge University, Cambridge, U.K., 1984.
(37) Miller, J. H. *Experiments in Molecular Genetics*; Cold Spring Harbor Laboratory Press: Cold Spring Harbor, NY, 1972.
(38) Fling, S. P.; Gregerson, D. S. *Anal. Biochem.* **1986**, *155*, 83–88.
(39) Gill, S. C.; von Hippel, P. H. *Anal. Biochem.* **1989**, *182*, 319–326.
(40) Voss, S.; Skerra, A. *Protein Eng.* **1997**, *10*, 975–982.

Me·*p*-NH_2-Bn−CHX-A″-DTPA chelate complex in the range 0.016−100 nM. In this case, the data were fitted to the sigmoidal equation

$$\dot{A} = \frac{\dot{A}_{max} - \dot{A}_{min}}{1 + \left(\frac{[L]_{tot}^{free}}{K_D}\right)^p} + \dot{A}_{min}$$

which contains the curve slope p (the Hill coefficient) as an additional parameter.

Measurement of Binding Activity for the Me·DTPA Group via Surface Plasmon Resonance. Real-time ligand-binding analysis of Lcn2 variants via surface plasmon resonance (SPR) was performed on a BIAcore X system (BIAcore, Uppsala, Sweden) using PBS/t [PBS containing 0.005% (v/v) Tween 20] as the running buffer. Solutions of the Me·DTPA−RNase conjugate (5−27 μg/mL in 10 mM sodium acetate, pH 5.0) were immobilized on a CM5 chip using standard amine-coupling chemistry, resulting in a ligand density of 300−1500 resonance units (RU). The purified Lcn2 variant was applied at a flow rate of 25 μL/min at concentrations of 0.5−320 nM. The sensorgrams were corrected by double subtraction of the corresponding signals measured for the control channel, which had been activated as above and blocked with ethanolamine, and an averaged baseline determined from several buffer blank injections.[41] Kinetic data evaluation was performed by a global fit of the traces from at least six different sample injections according to the 1:1 Langmuir binding model using BIAevaluation software, version 3.0.[42] For equilibrium binding analysis, stationary resonance signals 200 s after sample injection were plotted against the corresponding concentrations of the Lcn2 variant (see the Supporting Information). Curve fitting of these data points was performed as described for the ELISA.

Crystallization of Lcn2 Variants. After dialysis against 100 mM NaCl in 10 mM Tris/HCl (pH 8.0), the Lcn2 variants Tb7.14 and Tb7.N9 were concentrated to 18 and 25 mg/mL, respectively, using 10 kDa cutoff Ultrafree concentrators (Millipore, Billerica, MA) and sterile-filtered with a 0.45 μm Costar Spin-X centrifuge unit (Sigma-Aldrich). The proteins were crystallized using the sitting (Tb7.14) or hanging (Tb7.N9) drop vapor-diffusion technique.[43] For crystallization of Tb7.14, 0.25 μL of the solution of the apoprotein was mixed with 0.25 μL of reservoir solution [2 M $(NH_4)_2SO_4$, 200 mM Li_2SO_4, 100 mM Tris/HCl (pH 7.0)]. Crystals of space group $P4_12_12$ with three protein chains per asymmetric unit were obtained after 6 weeks at 20 °C. Tb7.N9 was crystallized at a final protein concentration of 22 mg/mL (1.1 mM) after addition of a slight excess of Y·DTPA−Tris (1.6 mM final concentration). In this case, 1 μL of protein/ligand solution was diluted with 1 μL of water and mixed with 1 μL of reservoir solution [22% (w/v) PEG 3350, 100 mM Bistris/HCl (pH 5.5)]. Crystals of space group $P4_12_12$ with two protein chains per asymmetric unit were obtained after 1 week at 20 °C. Crystals of the two Lcn2 variants were soaked in the corresponding precipitant solution supplemented with 30 and 20% (v/v) glycerol, respectively, prior to freezing in liquid nitrogen.

Data Collection and Model Building. Synchroton diffraction data for the Tb7.14 apoprotein and the Tb7.N9 ligand complex were collected using beamline 14.1 at Berliner Elektronenspeicherring-Gesellschaft für Synchrotronstrahlung (BESSY; Berlin, Germany). The data (Table 1) were processed with MOSFLM and scaled with SCALA.[44] Molecular replacement of the Tb7.14 apoprotein was carried out with the program EPMR[45] using the structure of wild-type Lcn2 (PDB entry 1X71).[12] Thereafter, molecular replacement of the liganded Tb7.N9 was carried out with the program MOLREP[44] using the refined model of Tb7.14.

The atomic models were built with the program O.[46] For Tb7.14, there was continuous electron density (at a resolution of 2.5 Å) for residues Ser3−Leu42 and Pro48−Gly178 of molecule 1, Ser3−Ala41 and Gln49−Asp177 of molecule 2, and Gln1−Leu42 and Pro48−Asp177 of molecule 3. For Tb7.N9, there was continuous electron density (at a resolution of 2.0 Å) for residues Leu7−Ala40 and Leu42−Gly178 of molecule 1 and residues Asp6−Ala40 and Leu42−Gly178 of molecule 2. The ligand Y·DTPA−Tris (resulting from the addition reaction between Tris and *p*-SCN-Bn−CHX-A″-DTPA) was modeled using Insight II (Accelrys, San Diego, CA) on the basis of the crystal structure of the plain In·DTPA complex (CSD entry MOQVOD),[47] and the corresponding topology and refinement parameters were generated using PRODRG.[48] Both crystal structures were refined with CNS,[49] and water molecules were added. Rotamers of Asn and Gln residues were checked with NQ-Flipper.[50] The refined structural models were validated with PROCKECK[51] and WHAT_CHECK.[52] Secondary structure was assigned using DSSP,[53] and protein/ligand contact surfaces were calculated with PISA.[54] Molecular graphics and structural superpositions were made with PyMOL,[55] while the protein/ligand interaction diagram was prepared with LIGPLOT[56] followed by manual adjustments. Both crystal structures were deposited at the RCSB Protein Data Bank (PDB) under the accession codes 3DTQ (Tb7.14) and 3DSZ (Tb7.N9).

Results

Selection of Variants with Me·DTPA Specificity from a Lipocalin Random Library. Starting from the known crystal structure of human Lcn2 complexed with its natural ligand enterobactin[5] and its cloned cDNA,[3] we constructed a combinatorial library by specifically randomizing the codons for 12 amino acid positions in the binding pocket (Figure 1C, Table 2). Residues at the bottom of the cavity and in close proximity to the bound iron siderophore complex, including two of the three positively charged side chains R81, K125, and K134 that are considered relevant for its recognition,[5] were preferentially chosen for the targeted mutagenesis. These positions were expected to tolerate both small- and large-side-chain substitutions, reaching as deeply as possible into the cavity without affecting the hydrophobic core packing in the lower part of the β-barrel.

Concerted random mutagenesis of these positions, which are distributed across a large part of the Lcn2 primary structure, was realized by means of a PCR assembly strategy (Figure 1D).

(41) Myszka, D. G. *J. Mol. Recognit.* **1999**, *12*, 279–284.
(42) Karlsson, R.; Michaelsson, A.; Mattsson, L. *J. Immunol. Methods* **1991**, *145*, 229–240.
(43) McPherson, A. *Crystallization of Biological Macromolecules*; Cold Spring Harbor Laboratory Press: Cold Spring Harbor, NY, 1999.
(44) Collaborative Computational Project, Number 4. *Acta Crystallogr., Sect. D: Biol. Crystallogr.* **1994**, *50*, 760−763.
(45) Kissinger, C. R.; Gehlhaar, D. K.; Smith, B. A.; Bouzida, D. *Acta Crystallogr., Sect. D: Biol. Crystallogr.* **2001**, *57*, 1474–1479.
(46) Jones, T. A.; Zou, J.-Y.; Cowan, S. W.; Kjeldgaard, M. *Acta Crystallogr., Sect. A: Found. Crystallogr.* **1991**, *47*, 110–119.
(47) Maecke, H. R.; Riesen, A.; Ritter, W. *J. Nucl. Med.* **1989**, *30*, 1235–1239.
(48) Schuttelkopf, A. W.; van Aalten, D. M. *Acta Crystallogr., Sect. D: Biol. Crystallogr.* **2004**, *60*, 1355–1363.
(49) Brünger, A. T.; Adams, P. D.; Clore, G. M.; DeLano, W. L.; Gros, P.; Grosse-Kunstleve, R. W.; Jiang, J. S.; Kuszewski, J.; Nilges, M.; Pannu, N. S.; Read, R. J.; Rice, L. M.; Simonson, T.; Warren, G. L. *Acta Crystallogr., Sect. D: Biol. Crystallogr.* **1998**, *54*, 905–921.
(50) Weichenberger, C. X.; Sippl, M. J. *Bioinformatics* **2006**, *22*, 1397–1398.
(51) Laskowski, R. A.; MacArthur, M. W.; Mos, D. S.; Thornton, J. M. *J. Appl. Crystallogr.* **1993**, *26*, 283–291.
(52) Hooft, R. W.; Vriend, G.; Sander, C.; Abola, E. E. *Nature* **1996**, *381*, 272.
(53) Kabsch, W.; Sander, C. *Biopolymers* **1983**, *22*, 2577–2637.
(54) Krissinel, E.; Henrick, K. *J. Mol. Biol.* **2007**, *372*, 774–797.
(55) DeLano, W. L. *PyMOL*; DeLano Scientific: San Carlos, CA, 2002.
(56) Wallace, A. C.; Laskowski, R. A.; Thornton, J. M. *Protein Eng.* **1995**, *8*, 127–134.

To this end, two gene segments, each comprising two of the total of four clusters of randomized residues (no. 1: 33, 36, 41; no. 2: 52, 54; no. 3: 68, 70, 79, 81; no. 4: 134, 136, 138), were first separately amplified using oligodeoxynucleotides with degenerate NNS codons at the desired positions. The two resulting PCR products, which included a short overlap in the middle of the Lcn2 gene, were isolated, mixed, and then assembled in another amplification with just a few cycles using flanking primers that contributed two unique *Bst*XI restriction sites. After unidirectional cloning on a phasmid vector suitable for filamentous phage display,[28] a molecular library with a diversity of $\sim 6.5 \times 10^{10}$ independent transformants was obtained.

This library was employed for the enrichment of Me·DTPA-specific Lcn2 variants via panning on ImmunoSticks coated with the immobilized ligand. For this purpose, a DTPA derivative with a chemically reactive isothiocyanate group, *p*-SCN-Bn−CHX-A″-DTPA, was covalently coupled to RNase, which served as a robust carrier protein devoid of nonspecific binding activities,[30] and charged with the transition metal ion Tb^{3+}. This lanthanide was chosen as a suitable central ion for the initial selection experiments as (i) it shows luminescent behavior that is strongly dependent on its molecular environment,[17,57,58] which was helpful for analyzing the proper charging of the protein−DTPA conjugate (see Materials and Methods), and (ii) its radius is not too different from those of therapeutically or diagnostically relevant radioactive isotopes such as $^{90}Y^{3+}$ and $^{177}Lu^{3+}$.[14,17]

After seven cycles of phagemid panning, the enriched pool of Lcn2 variant genes was subcloned onto another plasmid and subjected to a filter sandwich colony screen.[30] In this experiment, the Lcn2 variants were secreted from live *E. coli* colonies as a fusion with a bacterial ABD and became immediately bound to an underlying filter membrane coated with HSA. The functionally immobilized Lcn2 variants were probed for binding of an RNase double conjugate with Tb·DTPA and DIG groups. After signal development with an anti-DIG Fab/AP conjugate, several clones with specific ligand-binding activities were identified. Sequence analysis of 16 selected colonies revealed that seven of these carried an identical coding region, which was designated Tb7 (Table 2), while the remaining clones exhibited very similar sequences, having just four or fewer differing amino acids.

The Lcn2 variants were subcloned onto a suitable expression vector and produced as soluble proteins in the periplasm of the *E. coli* strain BL21, which lacks endogenous enterobactin,[5] or TG1-F^-. Purification from the periplasmic extract by means of the C-terminal *Strep*-tag II[33] and SEC yielded 1−6 mg of protein per 2 L shake flask culture (depending on the time point of induction), similar to what was described previously for recombinant wild-type Lcn2.[3] The purity was greater than 95% as determined by Coomassie-stained SDS-PAGE (Figure 2). The binding activity was first investigated in an ELISA for the Tb·DTPA−RNase A conjugate. The variant Tb7 showed a strong, metal-dependent signal with an apparent affinity in the low nanomolar range (74.5 ± 7.8 nM; Figure 2B), whereas wild-type Lcn2 exhibited no measurable signal in this assay.

Affinity Maturation of the Lcn2 Variant Tb7 for Improved Me·DTPA Binding. A second-generation library based on the coding region for the Lcn2 variant Tb7 was constructed by error-prone PCR of the central gene cassette (flanked by the two *Bst*XI restriction sites at amino acid positions 25−29 and 141−145) in the presence of deoxynucleotide analogues.[34] Next, four cycles of phagemid display and colony screening under more stringent conditions were carried out (see Materials and Methods). DNA sequencing of the 10 clones with the most intense signals for Tb·DTPA binding in the colony screen showed that nine of them carried the amino acid substitution Ile80Thr together with one or two additional substitutions at positions 65, 71, 73, 74, 75, 107, 116, or 135. The three variants Tb7.1 (Ile80Thr/Leu107Phe), Tb7.14 (Ile80Thr), and Tb7.17 (Phe71Ser/Lys73Glu/Ile80Thr) were again expressed as soluble proteins in *E. coli* BL21. After purification as described above, their ligand-binding properties were investigated in an ELISA (data not shown). These three variants exhibited somewhat higher signal intensities at saturation than Tb7, but their half-maximal concentration values for binding of the Tb·DTPA−RNase complex were not much improved.

In the second stage, site-specific saturation mutagenesis was performed in a consecutive manner for the amino acid sets at positions 79/80, 125/134, 125/127, 77/136, and 33/54/136, which were chosen according to the mutational pattern of the promising variants identified so far and molecular modeling on the basis of the Lcn2 structure as well as the crystal structure of its variant Tb7.14 (see below). To this end, a PCR assembly strategy similar to the one for the construction of the original library was applied, employing pairs of synthetic oligodeoxynucleotides carrying fully degenerate codon (or anticodon) sequences at the desired positions (see Materials and Methods). Since the resulting molecular libraries had low combinatorial complexities, they were directly subjected to the colony screen as before, except that lower ligand concentrations were used. Selection with randomized positions 79/80, 125/127, and 125/134 was performed with the Tb·DTPA−RNase−DIG conjugate, whereas for mutagenesis of positions 77/136 and 33/54/136 we applied the Y·DTPA−DIG conjugate, thus switching from Tb^{3+} to the medically more relevant Y^{3+}.

After each random mutagenesis, the gene cassettes of promising candidates were subcloned for periplasmic expression, and the best clone was identified using ligand affinity, yield of soluble periplasmic expression, and stable monomer formation during SEC as criteria. As a result of this procedure, three variants with improved binding activities successively emerged: Tb7.N9 (Ala79Leu/Ile80Thr), Tb7.N9.N34 (with the additional substitution Ser127Gln), and Yd5 (with the further substitutions Asp77Glu/Thr136Ser) (Table 2). The final variant, Yd5, showed the best binding activity, with an affinity improved by a factor of ~40 compared with Tb7 (see below and Table 3).

In the third stage, another error-prone PCR mutagenesis of the whole central coding cassette was performed on the basis of Yd5 and followed by phage display selection toward slow dissociation kinetics using competitive conditions. To this end, panning was carried out with the Y·DTPA−RNase target adsorbed to ImmunoSticks, and after a wash, bound phagemids were incubated for 30 min in the presence of a 500 μM solution of the free metal chelate complex Y·*p*-NH_2-Bn−CHX-A″-DTPA as a competitor; this was followed by further washing steps and, finally, acid elution. After three cycles of phagemid selection, the enriched pool of Lcn2 variants was subcloned and subjected to the colony screening assay, again applying competitive conditions (see Materials and Methods). The 16 variants that gave rise to intense staining signals, even in the presence of ~1000-fold higher molar concentration of the Y·DTPA

(57) Handl, H. L.; Gillies, R. J. *Life Sci.* **2005**, *77*, 361–371.
(58) Martini, J. L.; Tetreau, C.; Pochon, F.; Tourbez, H.; Lentz, J. M.; Lavalette, D. *Eur. J. Biochem.* **1993**, *211*, 467–473.

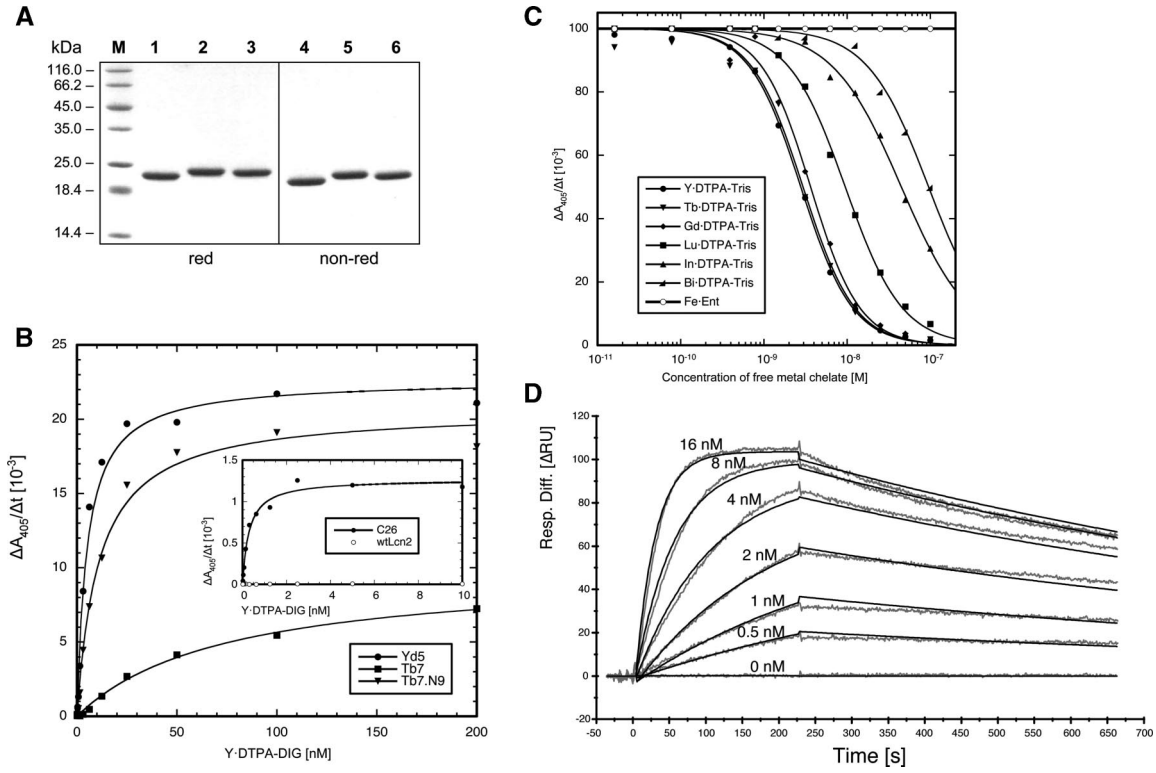

Figure 2. Properties of Lcn2 variants with Me·DTPA binding activity. (A) SDS-PAGE analysis of recombinant wild-type Lcn2 (lanes 1 and 4) and its variants Tb7.N9 (lanes 2 and 5) and C26 (lanes 3 and 6) after *Strep*-tag II affinity purification and gel filtration. Lanes 1−3 show samples reduced with 2-mercaptoethanol. The slightly enhanced electrophoretic mobility under nonreducing conditions (lanes 4−6) indicates proper formation of the single disulfide bond in each case. (B) Binding activity in the ELISA. A microtiter plate was coated with the purified Lcn2 variants (which were captured via an antibody specific for the *Strep*-tag II) and then incubated with a dilution series of the Y·DTPA−DIG (small-molecule) conjugate; incubation was followed by detection with anti-DIG Fab/AP and pNPP substrate. Recombinant wild-type Lcn2 revealed negligible signals in this assay. It should be noted that the Lcn2 variant from the final maturation step, C26 (see inset), was applied at a significantly lower density (100 vs 250 nM, with a capture antibody concentration of 1.8 vs 10 μg/mL). (C) Plain metal chelate binding activity of Lcn2 variant C26 in a competitive ELISA using various metal ions. The setup of this ELISA was similar to the one shown in panel (B) but used a fixed concentration (5 nM) of the Y·DTPA−RNase−DIG (protein) conjugate as tracer in the presence of a variable concentration of either the Me·DTPA−Tris chelate complex or (for comparison) Fe·enterobactin. (D) Real-time kinetic analysis of the Lcn2 variant C26 measured on a Biacore instrument. The Y·DTPA−RNase conjugate was coupled via amine chemistry to a CM5 sensor chip (ΔRU = 300), and the purified Lcn2 variant was applied at varying concentrations as indicated. The measured signal is shown as a gray line and the fitted curve as a black line in each case. The kinetic constants determined from this set of curves are listed in Table 3.

Table 3. Dissociation Constants and Binding Kinetics of Selected Lcn2 Variants for Y·DTPA−RNase Measured by Real-Time SPR Analysis

Lcn2 variant	k_{on} (10^6 M^{-1} s^{-1})	k_{off} (10^{-2} s^{-1})	K_D (nM) kinetic[a]	K_D (nM) equil.[b]	K_D (nM) ELISA[c]	$\tau_{1/2}$ (s)[a]
Tb7	1.06 ± 0.01	9.34 ± 0.08	88.3	89.4 ± 8.7	74.5 ± 7.8	7
Tb7.N9	2.17 ± 0.03	3.07 ± 0.02	14.2	17.1 ± 2.0	10.9 ± 1.3	23
Tb7.N9.N34	2.16 ± 0.03	2.98 ± 0.02	13.8	13.2 ± 1.5	n.d.	23
Yd5	2.53 ± 0.02	0.527 ± 0.003	2.08	3.78 ± 0.16	5.07 ± 0.72	132
C26	2.23 ± 0.01	0.0935 ± 0.0005	0.418	n.d.[d]	0.298 ± 0.044	741

[a] Determined from the k_{on}/k_{off} kinetic analysis (for the original sensorgrams, see Figure 2D and the Supporting Information). [b] Determined from equilibrium analysis of the SPR data (see Supporting Information). [c] Determined from the ELISA results depicted in Figure 2B. [d] Equilibrium analysis was not possible because the stationary association phase was not reached in the low concentration range investigated.

competitor, were sequenced, resulting in the identification of the variant C26, which exhibits five further mutations (Leu42Pro/Pro48Leu/Gln49Leu/Ile55Thr/Lys75Met), most of them in loop #1 (Table 2).

Biochemical Characterization of Selected Lcn2 Variants by Competitive ELISA and SPR. The Lcn2 variants resulting from the affinity maturation of Tb7 were produced in *E. coli* as soluble proteins at the shake-flask scale and purified via the *Strep*-tag II and SEC as before. All of the selected variants exhibited excellent expression characteristics and were purified as stable and fully monomeric proteins from the periplasmic cell extract (Figure 2A), showing final yields in the same range as for wild-type Lcn2 and the previously investigated variants.

The binding activities were first compared in an ELISA using the Lcn2 variants captured via an anti *Strep*-tag II antibody on the microtiter plate by incubating them with varying concentrations of the Y·DTPA−DIG conjugate, which was finally detected with an anti-DIG Fab/AP conjugate (Figure 2B). All of the variants ranging from Tb7 to its most improved derivatives showed hyperbolic saturation curves, whereas wild-type Lcn2 did not reveal any binding activity for the prescribed metal chelate complex. The amplitudes of the saturation curves increased while the half-maximal ligand concentrations, corresponding to the apparent K_D values (see Table 3), decreased over the course of the in vitro affinity maturation.

The binding activity for the small soluble metal chelate ligand was further investigated in a competitive ELISA using microtiter plates with the captured Lcn2 variants, employing Me·DTPA−RNase−DIG as the tracer and Me·DTPA−Tris as the free-ligand competitor, charged with Tb^{3+} or Y^{3+}. These measurements showed clear inhibition curves in case of the variants Tb7, Tb7.N9, and Yd5, and revealed a particularly high affinity for C26. This final variant was more thoroughly analyzed using a series of different metal ions (Figure 2C). Its K_D values deduced from the half-maximal free metal chelate concentrations after curve fitting were 2.77 ± 0.06 nM (Y^{3+}), 3.63 ± 0.20 nM (Gd^{3+}), 2.95 ± 0.18 nM (Tb^{3+}), 9.47 ± 0.34 nM (Lu^{3+}), 44.7 ± 2.5 nM (In^{3+}), and 95 ± 7 nM (Bi^{3+}). Thus, the engineered Lcn2 variants, especially C26, exhibit strong binding activity toward the small DTPA chelating group charged with different trivalent metal ions, whereas the context of RNase, which had been employed as a carrier protein during the selection, did not play a significant role. Notably, the main-group metal ions In^{3+} and Bi^{3+} seem to be recognized with significantly lower affinities compared with the lanthanide ions tested.

Finally, the Lcn2 variants were analyzed by SPR using a Biacore CM5 chip with the covalently attached Y·DTPA−RNaseA conjugate and applying the purified recombinant proteins (Table 3). Again, wild-type Lcn2 did not exhibit any significant binding activity, while moderate binding signals were obtained for Tb7. However, its derivatives isolated at different stages of the in vitro affinity maturation showed increasing affinity toward the immobilized target, with a value of ∼2 nM for Yd5, which represents ∼40-fold improvement over the parental variant. The smaller K_D values result primarily from slower ligand dissociation, with Yd5 showing quite a long half-life ($\tau_{1/2}$ = 132 s; Table 3). Notably, the variant C26 resulting from the final competitive selection experiment revealed in this assay an affinity of 418 pM for the metal chelate (Figure 2D), whereby its dissociation rate constant was further decreased by a factor of 5−6.

Crystallographic Analysis of Lcn2 Variants with Me·DTPA Binding Activity. The Lcn2 variants Tb7.14 and Tb7.N9 were successfully crystallized and their X-ray structures solved, the former as an apoprotein and the latter complexed with the ligand Y·DTPA−Tris. As expected, both proteins exhibit the typical lipocalin fold (Figure 3). Superposition of the individually refined protein chains with wild-type Lcn2 complexed with enterobactin (PDB code 1L6M) showed that the overall fold is extremely well-conserved despite the large number of amino acid exchanges (16). In particular, the β-barrel itself, the short loops at its closed end, the α-helix attached to its side, and even the more-or-less flexible N- and C-terminal extensions of the polypeptide chain are almost indistinguishable, although the three proteins were crystallized in a nonisomorphic manner and thus with different crystal packing neighborhoods.

Superposition of the 58 mutually equivalent backbone positions of Tb7.14 and Tb7.N9 (Cα atoms 28−37, 52−58, 63−69, 77−84, 91−94, 106−113, 118−124, and 133−139, each from chain A) that are structurally conserved for the β-barrel of the lipocalins[2] resulted in a root-mean-square deviation (rmsd) of 0.31 Å. For Tb7.14 and Lcn2, the rmsd was 0.23 Å, while the corresponding pairwise rmsd for Tb7.N9 and Lcn2 was 0.32 Å (both for chain A). Comparison of the side-chain conformations of Tb7.14 and Tb7.N9 revealed significant changes only for residues Gln33, Arg36, Gln49, Gln54, and Thr136. Among those, the side chain of Arg36 forms a hydrogen bond between its guanidinium NH1 atom and a carboxylate oxygen (O2) of the DTPA ligand (3.3 Å in the case of chain A).

In the complex with Tb7.N9, the bound Y·DTPA−Tris ligand nestles at one side of the cleft at the open end of the β-barrel and fills about one-third of its volume. The remainder of the cavity is occupied with nine water molecules, which form a hydrogen-bonding network. The DTPA moiety of the ligand, which is well-defined in the electron density (Figure 3B) and reveals the anticipated chirality,[23] can be described as a baseball glove with the metal ion representing the grabbed ball, similar to what was previously seen in the small-molecule crystal structure of an In^{3+}·DTPA complex.[47] The central Y^{3+} ion is coordinated by nine atoms. Eight of them stem from the octadentate chelating ligand [five of its carboxylate oxygens (with distances of 2.3−2.5 Å) and three of its amine nitrogens (with distances of 2.5−2.7 Å)], whereas one is a bound water oxygen (HOH1, with a distance of ∼2.9 Å). This water molecule is at hydrogen-bonding distance with two of the DTPA carboxylate groups (HOH1−LIG O1, 2.9 Å; HOH1−LIG O9, 3.0 Å) and with another crystallographically defined water molecule (HOH2, at a distance of 2.6 Å) in the second shell around the metal ion (Figure 3C), which itself is hydrogen-bonded to Ser134 (HOH2−Ser134 OG, 2.9 Å). Similar to the situation in the natural Lcn2/Fe·enterobactin complex, there are no direct liganding contacts between the metal ion and protein side chains.

The entire metal chelate complex is oriented with its hydrocarbon groups, as well as the cyclohexane ring and the benzyl side chain of the Bn−CHX-A″-DTPA derivative, directed toward a contiguous hydrophobic stretch of amino acid side chains on β-strands B, C, and D (Figure 3A,B). The polar carboxylate groups, as well as the Y^{3+}-coordinating water molecule, point toward β-strands G, H, and A, where a gap filled with further water molecules is formed that otherwise is occupied by the natural siderophore in the case of wild-type Lcn2. The thiourea group protruding from the benzyl side chain and its conjugated Tris moiety are oriented outward from the lipocalin cleft. There are two hydrogen bonds between atom N4 of the thiourea group and the two carboxylate oxygens of Asp77 (OD1 at a distance of 3.0 Å; OD2 at a distance of 3.8 Å). The terminal tris-hydroxymethyl substituent is only partially defined in the electron density.

Structural Comparison between Engineered and Natural Lcn2. The four loops at the open end of the β-barrel, which harbor most of the side-chain substitutions that were introduced when the ligand pocket was reshaped for the binding of Y·DTPA, have largely retained their geometry compared with the wild-type protein (Figure 3A). In particular, loops #2, #3, and #4, which connect β-strands C/D, E/F, and G/H, respectively, exhibit an unchanged conformation except for individual minor shifts of the loops as a whole. A maximum shift of ∼1.3 Å (after superposition of the 58 conserved Cα positions) is seen for the Cα position 73 at the tip of loop #2 in chain C of the apo-Tb7.14 structure, which may however reflect a crystal packing effect.

In contrast, the rather long Ω-type loop #1, which connects β-strands A/B, shows considerable backbone plasticity among the three different crystal structures, even though it is not involved in crystal packing contacts. Especially for chains A and C of the apo-Tb7.14 structure, this loop is almost identical with that of wild-type Lcn2 in the region around residue 46, while significant deviations occur at residue 41. However, in the case of chain B, the entire segment between

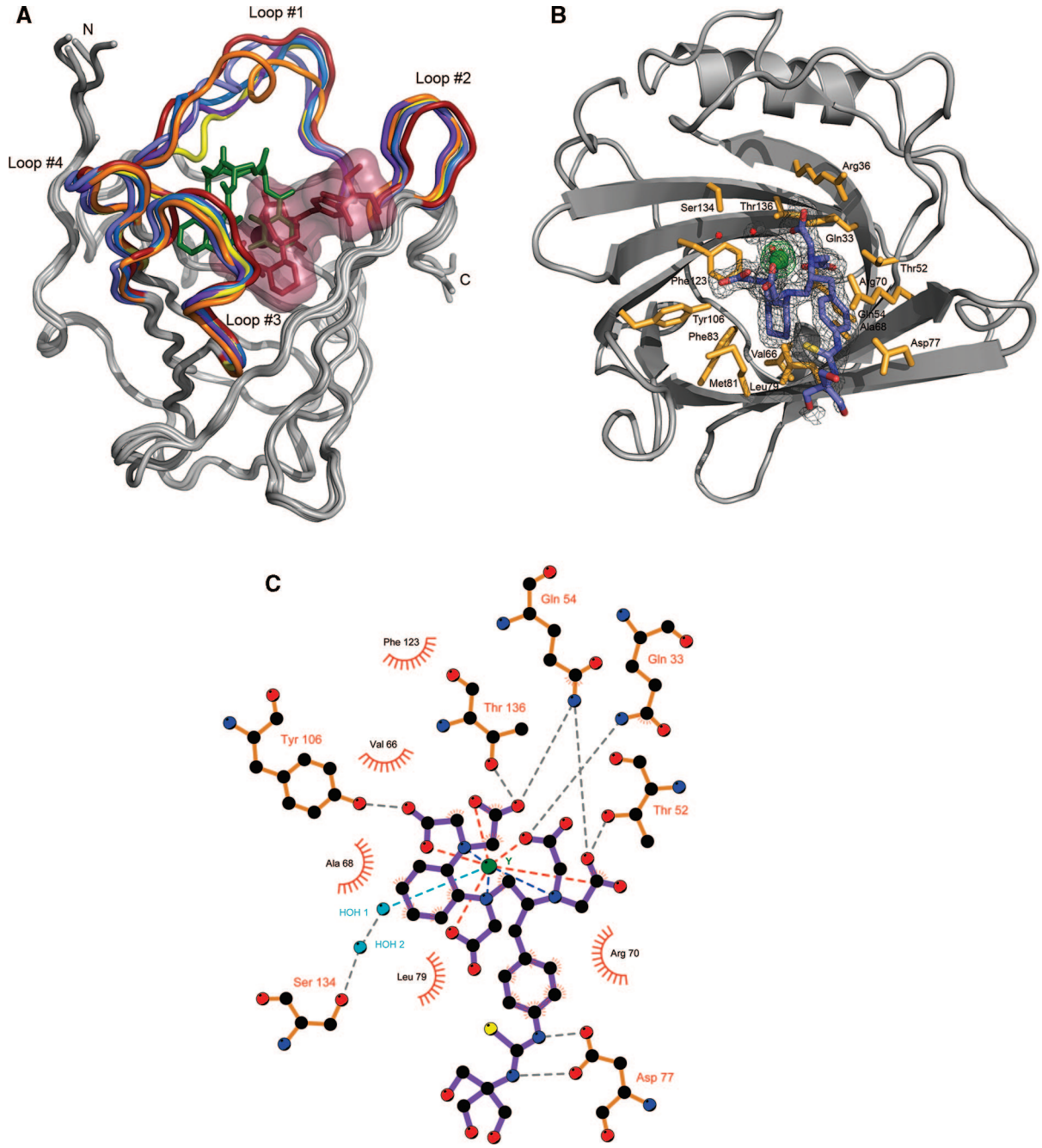

Figure 3. Crystal structure of Lcn2 variants with Me·DTPA binding activity. (A) Superposition of apo-Tb7.14 (chain A, marine; chain B, light-blue; chain C, violet) and the Tb7.N9/Y·DTPA−Tris complex (chain A, firebrick; chain B, orange) on the crystal structure of the Lcn2/Fe·enterobactin complex (yellow). The structures were superimposed using a set of 58 Cα positions that are conformationally conserved throughout the lipocalin family (28−37, 52−58, 63−69, 77−84, 91−94, 106−113, 118−124, and 133−139). The four loops at the open end of the β-barrel, which are structurally variable, are labeled. The Y·DTPA ligand is colored dark-red with a translucent surface, and the Y^{3+} ion is depicted as a black sphere. For comparison, the Fe·enterobactin ligand of Lcn2 (green) is also shown. (B) View into the cavity of Tb7.N9 with the bound Y·DTPA ligand, including its $2F_o - F_c$ electron density, which is contoured at 1σ around DTPA and the metal-coordinating water molecule (gray) and at 4σ around the Y^{3+} ion (green). Randomized positions and residues relevant during the affinity maturation are depicted in orange, while the second water molecule that forms the bridge to Ser134 is shown as a red sphere. (C) LigPlot representation of the chemical structure of the ligand Y·DTPA−Tris (with violet chemical bonds) and its molecular interactions when complexed with Tb7.N9 (hydrogen bonds, gray; coordination bonds to the central Y^{3+} ion, red, blue, and cyan). All of the residues shown were mutated in the course of Lcn2 engineering for the new ligand specificity, except Val66, Tyr106, and Phe123 (see Table 2).

residues 40 and 49 seems to be shifted by almost 5 Å (for the backbone). In the case of the two chains of the Tb7.N9/Y·DTPA complex that are present in the asymmetric unit, the shift is even more severe, with one turn of a 3_{10}-helix appearing for residues Arg43−Lys46 of chain B. Notably, there is missing electron density for parts of this loop, which is another indication of enhanced conformational flexibility. Consequently, the conformation of loop #1 seems to be influenced not only by the molecular environment but also by the presence of the metal chelate ligand. This behavior suggests that future mutational studies should be focused at loop #1 in order to achieve altered backbone conformations that may lead to better enclosure of the bound Y·DTPA ligand and possibly to even higher affinities.

In the crystal structure of the Tb7.N9 complex, the metal chelate is bound more deeply than the natural ligand enterobactin complexed with Lcn2, and it is situated almost in the middle between the 12 residues that were mutagenized in our original random library. The diethylenetriamino moiety interacts mainly with residues on β-strands C and D, whereby the cyclohexane ring packs against the hydrophobic residues Val66, Leu79, and Met81. On the other hand, the benzyl side chain is sandwiched between Arg70 and Leu79 and protrudes with its Tris substituent into the solvent. The entire cavity is positively charged, similar to wild-type Lcn2,[5] with the exception of the stretch formed by the residues Val111, Val121, and Phe123 at the bottom of the binding site. The larger side chain of residue Leu at position 79 compared with the one of Ala in the variant Tb7.14 leads to an improved van der Waals contact with the phenylthiourea group of the ligand.

Notably, Met81 has replaced Arg81 in Lcn2, which is one of the three positively charged side chains that were described to participate in cation$-\pi$ interactions with the bound Fe·enterobactin.[5] Its mate Lys134 is replaced by Ser, thus providing space for the Y^{3+} metal ion as well as for two of the DTPA carboxylate groups and the liganding water molecule. The more remote residue Lys125 of this triad may contribute to a general electrostatic interaction with the overall negatively charged metal chelate complex. In fact, this position was in some screens found to be occupied by Arg (data not shown).

Altogether, 15 residues are situated in contact distance (4 Å radius) with the bound metal chelate complex (Figure 3C), with at least one in each of the eight β-strands: Gln33, Arg36, Thr52, Gln54, Val66, Ala68, Arg70, Asp77, Tyr78 (only via backbone), Leu79, Met81, Phe83, Tyr106, Phe123, and Thr136. On the other hand, there are rarely any contacts between the bound metal chelate and the four loops. Despite the larger diameter of the prescribed ligand compared with Fe·enterobactin, this is possible because of its deeper burial within the lipocalin cavity. The buried surface area of Y·DTPA−Tris amounts to 621 Å^2, together with 442 Å^2 on the side of the protein (for chain A), which is significantly larger than the buried surface for Fe·enterobactin (429 Å^2) bound to Lcn2 (334 Å^2 for polypeptide chain A; calculated for PDB entry 1L6M).

Among those contact residues, nine positions were subject to mutagenesis in the initial Lcn2 random library (see Table 2). The substitution Asp77Glu was found at a later stage of affinity maturation, whereas only four of the contacting side chains (66, 83, 106, and 123) correspond to original residues of Lcn2. Interestingly, they still adopt the same rotamer conformations in the Y·DTPA complex. Apart from these minor structural remnants, the mode of binding to the engineered lipocalin is totally different for the Y·DTPA complex than for Fe·enterobactin bound to Lcn2.

Although the two crystal structures described here were obtained for Lcn2 variants at intermediate stages of the affinity maturation, at least some of the additional mutations acquired on the way to the final variant C26 can be rationalized on their basis (see Table 2). The substitution Ile80Thr, which was independently found in several screening experiments at the early stage of this project, occurs at a critical position between Leu79 and Met81 mentioned above. The Thr side chain is displayed on the outside of the β-barrel and seems to be slightly shifted compared with the original residue in Lcn2. The additional hydrogen bond between OG1 of Thr80 and OG1 of Thr67 locally stabilizes the pairing of strands C and D. Thus, this replacement may effect a local change in the backbone geometry.

The substitution Ser127Gln in variant Tb7.N9.N34 occurs at the tip of loop #4 and is remote from the bound ligand, which is in agreement with its marginal effect on the affinity (Table 3). In contrast, the conservative substitutions Thr136Ser and Asp77Glu observed for the variant Yd5 seem to improve polar contacts with one of the carboxylates and the thiourea group, respectively, of the bound Y·DTPA−Tris ligand (see Figure 3B,C).

Of the five additional side-chain replacements that were identified for the variant C26 (at positions 42, 48, 49, 55, and 75), three are located in loop #1 (residues 42, 48, and 49). These substitutions could lead to a gross conformational change and bring this loop closer to the ligand, as anticipated further above. The side chain at position 55 is situated on the outside of the β-barrel; as in the case of position 80, an Ile residue is exchanged for Thr, which may have a similar effect (mediated via the backbone) on the neighboring Gln54, which contacts the DPTA ligand. Finally, the replacement of Lys75 by Met occurs at the tip of loop #2, at the end of a stretch of three consecutive Lys residues, and may influence the interaction with the side chain of the Bn−CHX-A″-DTPA group via an electrostatic mechanism.

Discussion

Using targeted random mutagenesis and guided selection followed by a few cycles of affinity maturation, we were able to engineer human Lcn2 to recognize benzyl-substituted cyclohexyl-DTPA chelate complexes of Y^{3+} and related lanthanide ions. It is surprising that just 15 amino acid exchanges in the ligand pocket were sufficient to switch the specificity from the catecholate-type siderophore to this artificial ligand, yielding a K_D value of ~2 nM for the Lcn2 variant Yd5. A few more side-chain substitutions in the flexible loop #1 shifted the affinity even into the picomolar range for the advanced variant C26; this value is similar to the remarkably high affinity of wild-type Lcn2 for its natural ligand Fe^{3+}·enterobactin.[5] With this engineered lipocalin we have created a molecular docking module for chelated trivalent metal ions, including radioactive rare-earth elements relevant to nuclear medicine.

Compared with the historically important isotopes of iodine, radiometal ions have attracted increasing attention for radiolabeling tissue-specific antibodies or receptor-binding peptides because of their range of particle emissions, decay energies, and half-lives, which enable numerous applications. Their diverse properties permit adjustment to the pharmacokinetics and targeting behavior of the functional biomolecule and include both β- or α-emitting metal ions for medical therapy (RIT)[14] and γ or positron emitters for in vivo imaging (RID).[13,59]

In attempts to construct bispecific reagents, several antibodies have been raised against medically relevant metal chelate complexes. Structural information and precise affinity values are available for some of these, such as the Fab fragment 2D12.5 directed against complexes between Y^{3+} or Gd^{3+} and a functionalized DOTA[60] and the Fab fragment CHA255 directed against a complex between In^{3+} and a functionalized EDTA.[61]

(59) Gambhir, S. S. *Nat. Rev. Cancer* **2002**, *2*, 683–693.
(60) Corneillie, T. M.; Fisher, A. J.; Meares, C. F. *J. Am. Chem. Soc.* **2003**, *125*, 15039–15048.
(61) Love, R. A.; Villafranca, J. E.; Aust, R. M.; Nakamura, K. K.; Jue, R. A.; Major, J. G., Jr.; Radhakrishnan, R.; Butler, W. F. *Biochemistry* **1993**, *32*, 10950–10959.

Interestingly, in both cases the binding mode of the chelate complex in the antibody combining site is different from the one observed here for the engineered lipocalin.

In both antibodies, the polar carboxylate groups of the chelator that coordinate to the metal ion point toward the bottom of the binding site while its aliphatic backbone appears at the entrance, forming contacts with aromatic side chains in the hypervariable loops, and the functional benzyl side chains are barely involved in protein contacts. Although the chemical structure of the chelator is unrelated, the binding of Fe^{3+}•enterobactin to wild-type Lcn2 is similar. There, the three catecholate groups that coordinate to the iron ion point into the cavity of the lipocalin while the triserine lactone backbone protrudes from its entrance. In contrast, the interaction between the engineered Lcn2 and the functionalized DTPA has a less polar nature but seems to be driven by tight hydrophobic contacts involving both the cyclohexyl and benzyl groups attached to the DTPA backbone.[23]

In this way, a picomolar affinity has been realized, which is significantly better than the ~10 nM affinity reported for the antibody recognizing Y^{3+}•benzyl-DOTA,[62] for example. Corresponding Fab fragments have been proposed as molecular docking stations for medical applications in pretargeting RIT. According to this strategy, the Fab fragment, linked to a tumor-specific antibody, is first targeted to the malignant tissue, and after excess protein is cleared from circulation, the radiometal chelate complex is applied. This small compound, which shows rapid diffusion, becomes captured at the disease site, whereas excess free reagent is quickly cleared from circulation via the kidney, thus leading to a high contrast for imaging or a high specific radiation load for therapy.[62] Unfortunately, the coupling of a radionuclide-binding Fab fragment with a tumor-specific antibody (via chemical conjugation, as a fusion protein or by production of a bispecific monoclonal antibody) is still difficult, and such attempts have remained scarce.

On the other hand, lipocalins with engineered ligand specificities, the so-called "anticalins", are much more amenable to the production of fusion proteins because of their composition as a single polypeptide chain with a robust fold and small size.[21] In fact, anticalins have been successfully fused with enzymes, other anticalins (yielding "duocalins"), and antibody fragments. Consequently, our Me•DTPA-specific Lcn2 variant provides a promising module for incorporation into novel biomolecular pretargeting reagents.

The results of our competition ELISA indicate that DTPA chelate complexes are recognized with varying affinities depending on the trivalent central ion. The slightly more pronounced discrimination between different metal ions compared with that of a Me•DOTA-specific Fab fragment[17] may be a consequence of the more open structure of the noncyclic DTPA chelate and its relaxed steric properties. Nevertheless, four lanthanide ions useful for nuclear medicine are among the ones that are most tightly bound by the engineered lipocalin: Y^{3+}, Tb^{3+}, Gd^{3+}, and Lu^{3+}. The β-emitter ^{90}Y is widely applied for radiotherapy,[14] whereas the isotope ^{86}Y is suitable for positron emission tomography.[60] The combined β/γ-emitter ^{177}Lu offers application for both radiotherapy and imaging.[14,15] Furthermore, the nonradioactive isotopes of Gd^{3+} and Tb^{3+} are of interest for magnetic resonance imaging and applications involving lanthanide luminescence, respectively.

One problem that persists in all metal-chelate-capturing approaches, whether mediated by cognate antibody fragments or the engineered lipocalin, pertains to the kinetic stability of the resulting biomolecular complexes. For example, the half-lives for dissociation of the Fab fragment complexes CHA255/In•EDTA and 2D12.5/Y•DOTA were both reported to be significantly less than 1 h, which is more than 1 order of magnitude smaller than the half-life for radioactive decay of the bound isotopes; thus, much of the specific energy load is lost via dissociation.[62] A similar situation occurs for the DTPA-specific lipocalin, which has a dissociation half-life of 12 min (as determined for the variant C26 in real-time SPR analysis).

To circumvent this general limitation, the concept of covalent (i.e., irreversible) complex formation, which is based on the incorporation of a moderately electrophilic group (e.g., acrylamide) into the chelate ligand, has been proposed. Sterically favorable introduction of a Cys residue into the binding site of the antibody, for example, may then lead to efficient Michael addition upon complex formation.[62] This strategy should be feasible for our engineered lipocalin, too. In fact, natural Lcn2 already exhibits an unpaired Cys residue (although its position would have to be shifted closer to the ligand pocket), and a Michael acceptor derivative of CHX-A″-DTPA was recently described.[63]

Apart from that, an even more general mechanism to make binding events less reversible takes advantage of the avidity effect. This concept is already in use for pretargeting RIT to achieve longer residence times. Especially in cases of high surface density of the tumor marker, bound bispecific antibodies have been (noncovalently) cross-linked with bivalent haptens.[15] Indeed, bivalent derivatives of the DTPA group were also synthesized and successfully applied in this context.[16] Thus, the preparation of fusion proteins between our Me•DTPA-specific anticalin and suitable targeting modules, in combination with bivalent metal chelates, might offer new prospects for pretargeting imaging and therapy.

In conclusion, on the basis of the successful example presented here, Lcn2 should provide a promising scaffold for engineering binding proteins for other metal complexes as well. These may be applied either for nuclear medicine (e.g., if directed against the Me•DOTA group) or for antiinfective therapy (e.g., if recognizing pathogen-related siderophores).

Acknowledgment. This work was supported by the Forschergruppe 411 and the Munich Center for Integrated Protein Science (CIPS-M), both funded by the Deutsche Forschungsgemeinschaft. The authors thank Walter Stelzer for MS analysis; Uwe Müller, Martin Fuchs, and Jörg Schulze for assistance in using beamline 14.1 at BESSY; and Free University Berlin at BESSY, whose support is gratefully acknowledged. The synchrotron measurements were supported by the BMBF (project funding reference number 05ES7BZA).

Supporting Information Available: Additional sensorgrams as well as equilibrium analyses of the SPR measurements for the Lcn2 variants listed in Table 3. This material is available free of charge via the Internet at http://pubs.acs.org.

JA806857R

(62) Corneillie, T. M.; Whetstone, P. A.; Meares, C. F. *J. Inorg. Biochem.* **2006**, *100*, 882–890.

(63) Xu, H.; Baidoo, K. E.; Wong, K. J.; Brechbiel, M. W. *Bioorg. Med. Chem. Lett.* **2008**, *18*, 2679–2683.